

Exchange energies of Kapellasite from high-temperature series analysis of the kagome lattice J_1 - J_2 - J_d -Heisenberg model.

B. Bernu,¹ E. Kermarrec,² C. Lhuillier,¹ F. Bert,² and P. Mendels^{2,3}

¹*LPTMC, UMR 7600 of CNRS, Université Pierre et Marie Curie, Paris VI, F-75252 Paris Cedex 05, France*

²*Laboratoire de Physique des Solides, Université Paris Sud 11, UMR CNRS 8502, F-91405 Orsay, France*

³*Institut Universitaire de France, 103 bd Saint-Michel, F-75005 Paris, France*

(Dated: October 10, 2012)

We present an analysis of the magnetic susceptibility and specific heat data of Kapellasite ($\text{Cu}_3\text{Zn}(\text{OH})_6\text{Cl}_2$) through high-temperature expansions (HTE) of the J_1 - J_2 - J_d -Heisenberg model on the Kagome lattice (up to order 9). Experimental data are reproduced with exchange energies $J_1 = -12.4(2) \text{ K}$ and $J_2 = -5.0(8) \text{ K}$ and $J_d = +14.8(8) \text{ K}$, where J_d is the third neighbor exchange energy across the hexagon. The agreement between theory and experiment is excellent for the spin susceptibility down to 20 K . Analysis of the spin specific heat data shows a deficit of 10% of the entropy around 10 K . This improved modeling confirms the results of ref³ regarding the location of Kapellasite in the cuboc2 phase of the Heisenberg model. The quality and limits of this modeling are discussed.

PACS numbers: 02.60.Ed 71.70.Gm 75.10.Kt 75.30.Et

I. INTRODUCTION

Kapellasite first synthesized in London^{1,2} is a polymorphous of Herbertsmithite of chemical formula $\text{Cu}_3\text{Zn}(\text{OH})_6\text{Cl}_2$. Contrary to Herbertsmithite, the susceptibility of this new metastable compound points to a ferromagnetic Curie Weiss field of about 10 K . Kapellasite was not found to develop dominant ferromagnetic correlations down to the lowest temperature and this information is the landmark of competing interactions. As this compound fails to develop any order down to 20 mK ³ a quantitative discussion of the possible spin liquid properties needs a modeling of the spin hamiltonian. Such a model could be built by successive approximations from a fit of the thermodynamic quantities to high temperature series expansions for a relevant set of hamiltonians. The actual chemical formula of the synthesized compound, determined with neutron powder diffraction², is $(\text{Cu}_{0.73}\text{Zn}_{0.27})_3(\text{Zn}_{0.88}\text{Cu}_{0.12})(\text{OH})_6\text{Cl}_2$, with 27% Zn on the Cu-sites of the kagome lattice and 12% Cu on the hexagonal Zn site. The Cu/Zn mixing leads to some disorder within the kagome planes but cannot induce any coupling between the planes, which occurs only via very weak O-H-Cl hydrogen bonds². Kapellasite is therefore remarkably two-dimensional.

A first theoretical description of Kapellasite, which is deep in the Mott phase, is the Heisenberg Hamiltonian on the perfect kagome lattice:

$$\mathcal{H} = \sum_{\langle i,j \rangle_\alpha} J_\alpha \mathbf{S}_i \cdot \mathbf{S}_j, \quad (1)$$

where the exchange integrals J_α are defined in Fig. 1. Due to the geometry of the exchange paths J_3 and J_d are different and J_d is expected to be larger than J_3 by an order of magnitude⁵. We will thus limit this first analysis to a pure J_1 - J_2 - J_d -model, neglecting both the effects of disorder and of an eventual Dzyaloshinskii-Moriya interaction. These issues will be discussed in the conclusion.

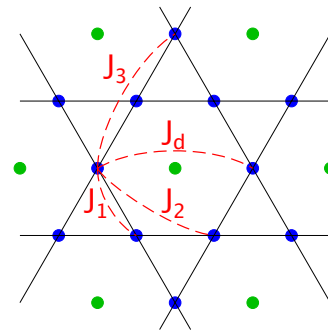


FIG. 1. (Color online) Kagome plane of Kapellasite with Cu^{2+} $S = 1/2$ spins (blue), non-magnetic Zn^{2+} ion (green), and exchange interactions (red).

Because of the competition between these various exchanges, the shape of the susceptibility and heat capacity versus T curves deviates noticeably from those of the pure Heisenberg model. In fact the 17th order HT series expansions of the nearest neighbor Heisenberg hamiltonian⁶ deviates significantly from the kapellasite data for temperatures lower than 70 K . We thus compute the HT series of magnetic susceptibility χ and specific heat C_v with the J_1 - J_2 - J_d parameters up to order 9 (see appendix A).

The paper is organized as follows. In section II, the magnetic susceptibility χ is fitted to experimental data providing strong constraints on the coupling constants. Section III is devoted to the specific heat analysis allowing us to further refine these constraints. Section II and III are organized similarly. We first detail the technicalities of the fits and finish with the physical conclusions to be kept in mind for the appreciation of the physical properties of the model. In the conclusion we discuss the consequences of neglecting at this stage the chemical disorder in the plane and Dzyaloshinskii-Moriya interactions.

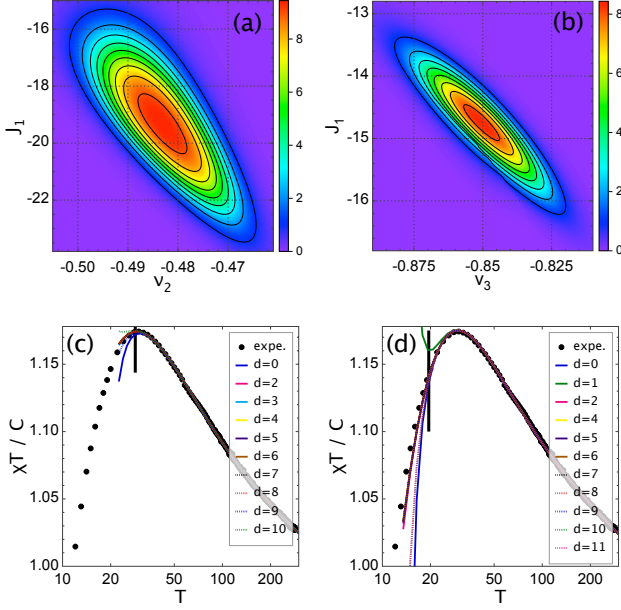


FIG. 2. (a) and (b): Fit quality, as defined by Eq.6 with $\epsilon = 10^{-3}$, versus ν_2 (a) or ν_3 (b) for $T_{\min} = 28.5 K$ (a) and $T_{\min} = 19.5 K$ (b). Contour levels are at integer values. The best fit is for the highest value of $Q_{\mathcal{X}}$ (thus in red). The best points are $\{J_1, \nu_2, A, B\} = \{-19.34 K, -0.483, 1.012, -6.5 \times 10^{-5} K^{-1}\}$ (a), $\{J_1, \nu_3, A, B\} = \{-14.74 K, -0.850, 1.023, -9.1 \times 10^{-5} K^{-1}\}$ (b). (c) and (d): comparison with experiment for these best points of (a) and (b) respectively. All PPAs at order $n = 10$ (c) $n = 11$ (d) are shown and d indicates the degree of the denominator for each PPA (see Appendix B for the PPA's definition). The thick vertical line indicates T_{\min} .

II. DESCRIBING $\chi(T)$

The dc susceptibility was measured in a commercial Quantum Design MPMS-5S SQUID magnetometer. Whereas a divergent behavior of χ is commonly observed in most frustrated magnets and interpreted as a signature of weakly coupled magnetic defects⁷, here, the NMR local probe data indicate that the measured macroscopic susceptibility is intrinsic. The experimental data are given as a list of points $\{T_k, \chi_k^{\text{exp}}\}$. Fitting the data to a Curie-Weiss law $\chi(T) \simeq C/(T - T_0)$, leads to $C = 0.429(2) \text{ cm}^3 K/\text{mol}$ and $T_0 = 9.5 \pm 1 K$, where T_0 is interpreted as the Curie-Weiss temperature. In the range of temperature of interest $\chi T/C$ is of order of unity and is thus a good quantity to fit.

We define the HT-series expansion of the magnetic susceptibility χ^{HT} :

$$\frac{\chi^{\text{HT}}(T)T}{C} = 1 + \sum_{i=1}^n P_i(J_1, J_2, J_d)\beta^i, \quad (2)$$

where $\beta = 1/T$ and P_i is an homogeneous polynomial of order i and n is the highest order at which the series

is known. $P_1(J_1, J_2, J_d) = \theta$ and for the Kagome lattice $\theta = -J_1 - J_2 - J_d/2$. Assuming $J_1 \neq 0$, we use as parameters $\nu_2 = J_2/J_1$ and $\nu_3 = J_d/J_1$ instead of J_2 and J_d , and define the polynomials $p_i(\nu_2, \nu_3)$ (see Appendix A) as:

$$\frac{\chi^{\text{HT}}(T)T}{C} = \sum_{i=0}^n \frac{p_i(\nu_2, \nu_3)}{i!} \left(\frac{J_1}{2T}\right)^i, \quad (3)$$

In order to account for the uncertainties in the number of spins and the temperature independent Van Vleck and diamagnetic susceptibilities, we introduce two parameters A (close to 1) and B and define a least mean square error as:

$$Z_{\mathcal{X}} = \sum_{k=1}^{N_T} \left[A \sum_{i=0}^n p_i(\{\nu_a\}) \left(\frac{J_1}{2T_k}\right)^i + BT_k - \frac{\chi_k^{\text{exp}} T_k}{C} \right]^2 \quad (4)$$

$$R_{\mathcal{X}} = \sqrt{Z_{\mathcal{X}}/N_T} \quad (5)$$

where N_T is the number of experimental measurements with $T \geq T_{\min}$, $T_1 \equiv T_{\min}$ is the lowest temperature included in the fit and $R_{\mathcal{X}}$ is a fit-error measure. One could minimize $R_{\mathcal{X}}$ with respect to the parameters $\{A, B, J_1, \nu_2, \nu_3\}$ taking advantage of the two linear parameters A and B . But using Pade approximants, allows to extend the fits to lower temperatures.

In the present method the best set of parameters is searched amongst that having the largest number Pade approximants providing a “good fit”, i.e. the lowest $R_{\mathcal{X}}$ error for the largest interval of temperatures. We thus define a measure of the fit quality as:

$$Q_{\mathcal{X}} = \sum_{\{\text{PPA}\}} Q_{\mathcal{X}, \text{PPA}} \quad (6)$$

$$Q_{\mathcal{X}, \text{PPA}} = \frac{1}{1 + (R_{\mathcal{X}, \text{PPA}}/\epsilon)^r} \quad (7)$$

where the sum runs over the *Physical Pade Approximants* (PPA), see appendix B, $\epsilon = 2 \times 10^{-3}$ is of the order of the experimental uncertainties while the parameter r controls how much the values outside of the uncertainties ϵ do contribute to $Q_{\mathcal{X}}$. A large value of r enforces the weight of “good” PPAs while it discards more rapidly the worse ones (here, $r = 8$). $R_{\mathcal{X}, \text{PPA}}$ is defined by replacing the HT-polynomial by a PPA in $R_{\mathcal{X}}$ (see Eq.4). If a PPA goes through all the experimental points, then $Q_{\mathcal{X}, \text{PPA}}$ is of the order of unity. On the other hand, if the PPA is “bad”, $R_{\mathcal{X}, d^*}/\epsilon$ is much larger than 1 and the contribution to $Q_{\mathcal{X}, \text{PPA}}$ will be small. Thus $Q_{\mathcal{X}}$ counts roughly the number of “good” PPAs. For $T_{\min} > 25 K$ we find that $Q_{\mathcal{X}}$ is very close to $n + 1$, i.e. each pade approximant is a PPA and $R_{\mathcal{X}, \text{PPA}} < \epsilon$. A large domain of parameters provides similar quality for the fits. This domain is restricted by using smaller values of T_{\min} .

Unfortunately, a minimization algorithm is not applicable because the function $Q_{\mathcal{X}}$ is not continuous (see appendix B) and has many local minima. On the other

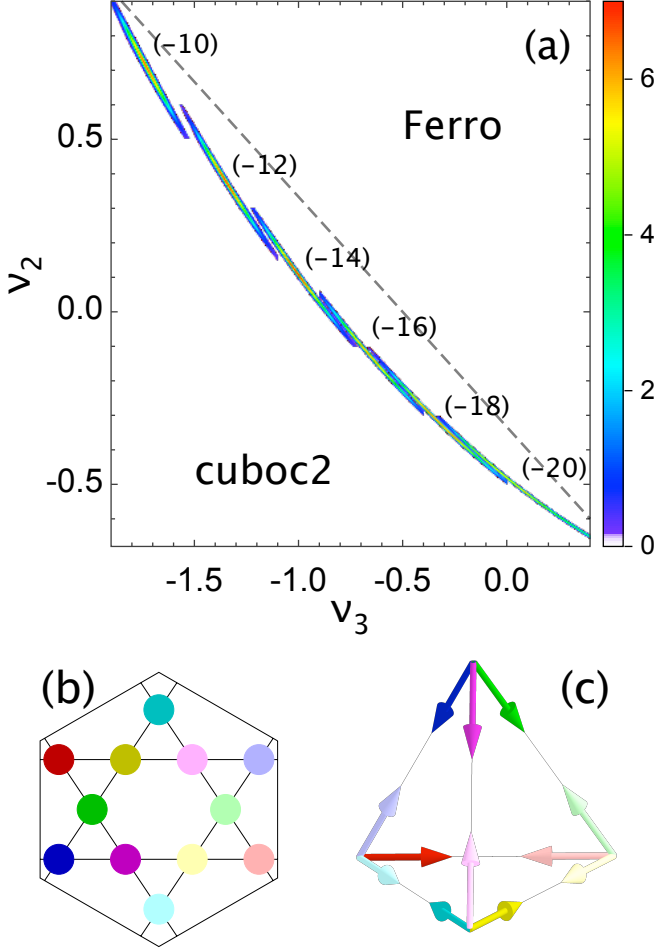


FIG. 3. (a): Fit quality, as defined by Eq.6 with $\epsilon = 10^{-3}$, versus ν_3 and ν_2 for $T_{\min} = 19.5 K$. The different narrow domains correspond to the values of J_1 given in parenthesis. The dashed line separates the ferromagnetic phase from the cuboc2 phase of the corresponding classical Heisenberg model. Note that the corresponding $\theta = -J_1(1 + \nu_2 + \nu_3/2)$ varies from $-8.4 K$ to $-10.4 K$ from the top-left solution to the down-right one. (b) and (c): the twelve sublattice-cuboc2 classical structure: the spins of a triangle in (b) start from (or arrive to) a summit of the tetrahedron in (c). Spins around an hexagon are on a facet of the tetrahedron and spins across an hexagon (J_d interaction) are on the same side of the tetrahedron, thus anti-parallel.

hand, as the number of parameters is reduced, the quality function Q_X can be evaluated on grids and after some trials the main minimum is eventually found.

At high temperature, almost all PPAs coincide with the HT-polynomial. As the temperature decreases, the PPAs start to deviate from each other or deviate from the experimental data and thus the quality of the fit decreases. As the function $Q_X(T_{\min})$ decreases sharply at some T_c , in the following T_{\min} is chosen just above T_c .

At fixed $\{J_1, \nu_2, \nu_3\}$, the polynomials $p_i(\nu_2, \nu_3)$ are

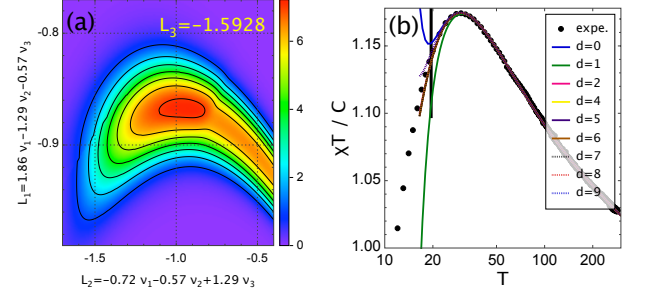


FIG. 4. (a): Fit quality, as defined by Eq.6 with $\epsilon = 10^{-3}$ with $T_{\min} = 19.5 K$. The linear relations are defined by Eqs.8-9 with the parameters reported in Table II. (b): Comparison with experiments where all PPAs are drawn.

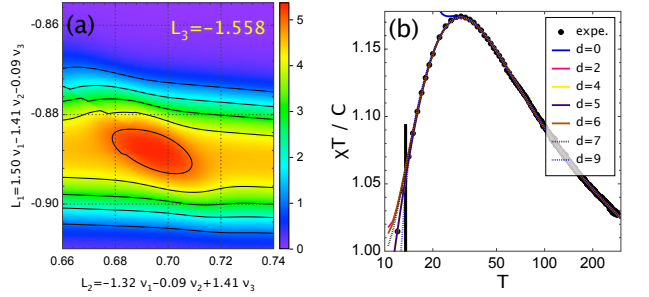


FIG. 5. Same as Fig.4 with $T_{\min} = 13.5 K$.

evaluated to numbers and $\chi^{HT}T/C$ becomes a polynomial of $\beta = 1/T$ only. Then all PPAs are computed (see appendix B). The parameters A and B must be kept fixed for all PPAs and their calculations are explained in Appendix C. Thus for a set of given coupling constants a value of Q_X is computed and we can look for the best coupling constant set.

The pure kagome model $\{J_1, 0, 0\}$ where the series is known at order 17 is compatible with the experimental data with ferromagnetic $J_1 \sim -12 K$, $A = 1.037$, $B = -1.2 \times 10^{-4} K^{-1}$ but only for $T > 70 K$. Then we check the models $\{J_1, \nu_2, 0\}$ and $\{J_1, 0, \nu_3\}$ where the polynomial has been computed up to order 10 and 11 respectively (see Appendix A). Fig. 2-(a)-(b) shows Q_X while Fig. 2-(c)-(d) shows all PPAs at the best points of (a)-(b). The fits are of similar quality but for model $\{J_1, \nu_2, 0\}$ T_{\min} is significantly higher. This is not because the series is known at higher order but because the shape of χT around the maximum is different. Note that for these two models J_1 is ferromagnetic while ν_2 (or ν_3) is negative, thus J_2 (or J_d) are anti-ferromagnetic. In each case the precision on ν_i is an order of magnitude better than for J_1 .

The next model involves $\{J_1, \nu_2, \nu_3\}$. Fig.3 shows Q_X for various values of J_1 as a function of ν_2 and ν_3 . We first see that for each J_1 only a narrow region leads to good

T_{\min}	19.5 K	13.5 K
ϕ	-1.2	-0.85
L_1	-0.867(3)	-0.888(2)
L_2	-0.93(5)	+0.695(5)
L_3	-1.5928(5)	-1.5580(15)
A	1.023	1.017
B	$-9.1 \times 10^{-5} K^{-1}$	$-7.6 \times 10^{-5} K^{-1}$
J_1	-13.76(15) K	-17.89(4) K
ν_2	+0.138(20)	-0.300(2)
ν_3	-1.042(25)	-0.364(3)
J_2	-1.9(3) K	+5.37(4) K
J_d	+14.4(5) K	+6.51(7) K
θ	8.5(5) K	-9.3(1) K
J_{CV}	10.5(3) K	11.78(4) K

TABLE I. Results of the fits of Fig.4,5. Errors on L_i are determined from the localization of the maximum to within 0.01. θ and J_{CV} are the coefficients of the leading term of the magnetic susceptibility and specific heat at high temperature.

fits. However, it is clear that two combinations of the parameters are strongly constrained. For example, we see that in each map, the maxima are near a line $\nu_2 + \nu_3 = f(J_1)$, with $f(J_1) \approx -a J_1 - 1.5$, with $a = 0.05 K^{-1}$. In order to capture the best domain, we change variables using an orthogonal transformation:

$$\begin{pmatrix} L_1 \\ L_2 \\ L_3 \end{pmatrix} = M \times \begin{pmatrix} \nu_1 = aJ_1 \\ \nu_2 \\ \nu_3 \end{pmatrix} \quad (8)$$

where ν_1 is dimensionless. In this equation $M = \mathcal{R} \times \mathcal{T}$ is a 3×3 matrix, where \mathcal{T} defines a new orthogonal basis with $L_3 = \nu_1 + \nu_2 + \nu_3$ and two orthogonal vectors to L_3 , while \mathcal{R} is a rotation of these two vectors around L_3 :

$$\mathcal{R} = \begin{pmatrix} \cos \phi & \sin \phi & 0 \\ -\sin \phi & \cos \phi & 0 \\ 0 & 0 & 1 \end{pmatrix} \quad \mathcal{T} = \begin{pmatrix} 0 & -1 & 1 \\ -2 & 1 & 1 \\ 1 & 1 & 1 \end{pmatrix} \quad (9)$$

where ϕ is chosen to obtain a domain $\{L_1, L_2\}$ as compact as possible. For fixed L_3 , $Q_{\mathcal{X}}$ is computed for a range of values for L_1 and L_2 . Figure 4-(a) shows $Q_{\mathcal{X}}$ at the best L_3 while 4-(b) shows the comparison with the experimental susceptibility at the best parameters for $T_{\min} = 19.5 K$. Values of the parameters and results for the best solutions are given in Table II. If we extend the fits to lower temperatures, a second point emerges, not as good around the maximum of $\mathcal{X}T$. Fig.5 shows this second possible solution. With this procedure we find two relations between the exchange energies which are known with good precision (L_1 and L_3) while a large uncertainty remains on the last one (L_2).

We finish this section with a few remarks: *i*) the uncertainty in the number of spins, measured here by A in Eq.4, is about 2% a value in agreement with experimental estimates. This shows that this model is realistic. *ii*) The Van Vleck and diamagnetic susceptibilities, B in Eq.4, less than $10^{-4} K^{-1}$, is also of the order of experimental uncertainties. *iii*) both θ and T_0 have a

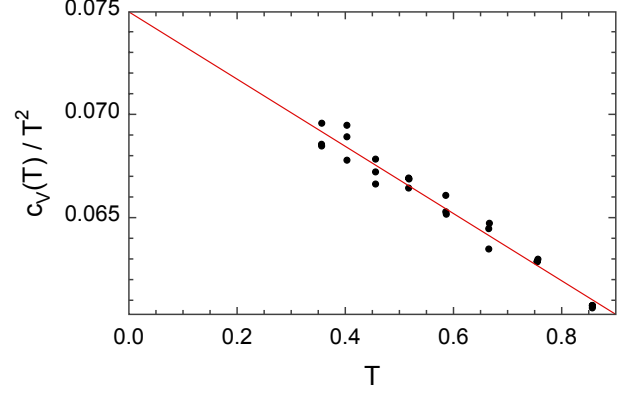


FIG. 6. Low temperature behavior of the Kapellasite specific heat. Points are experimental data and the line is a linear fit.

positive sign usually pointing to a ferromagnetic phase, but all the solutions found in this section fall in the anti-ferromagnetic Cuboc2 domain of the classical phase diagram of the J_1 - J_2 - J_d model; *iv*) the values of θ found with the high order fit and T_0 coming from the simple Curie-Weiss law differ slightly, due to neglecting the Van Vleck and diamagnetic susceptibilities (B in Eq.4) in the Curie-Weiss law; *v*) the fit of the spin susceptibility alone does not determine uniquely the three parameters of the model but constrains them strongly (see Fig.3).

III. DESCRIBING $C_V(T)$

Experimental data are given as a list of points $\{T_k, C_{V,k}^{\text{exp}}\}$. At high temperature, the leading term of the spin specific heat decreases as J_{CV}^2/T^2 , where J_{CV}^2 is a positive quadratic form of the coupling constant $\{J_a\}$, here $J_{CV}^2 = 3/8(J_1^2 + J_2^2 + J_d^2/2)$. On the other hand, at low temperature, the phonon-specific heat starts as $(T/T_D)^3$, where T_D is a Debye temperature. When J_{CV} is much smaller than T_D , as for helium-3⁴, each term can be evaluated separately. A quick analysis of the Kapellasite phonon specific heat reveals that $T_D \sim 160 K$ whereas, according to the results found in the previous section, $J_{CV} \sim 10 K$. Thus, between 10 and 100 K, both contributions are of the same order of magnitude. In this section, we analyze the spin specific heat at sufficiently low temperature such that the phonons can be neglected.

In the following c_V denotes the specific heat per spin. The experimental specific heat per spin is:

$$c_V^{\text{exp}}(T) = \frac{C_{V,\text{mol}}^{\text{exp}}(T)}{N_s k_B} \quad (10)$$

where N_s is the number of spin per mole. The leading low-temperature behavior of the specific heat (essentially

a spin contribution) is assumed to be:

$$c_V(T) = c_0 T^\alpha + \mathcal{O}(T^{\alpha+1}) \quad (11)$$

Fig-6 shows polynomial fits with experimental data of the Kapellasite, using $\alpha = 2$ as expected for a two-dimensional anti-ferromagnet and compatible with a cuboc2 structure found in the previous section. We find the extrapolated value at $T = 0$ of $c_V^{\text{exp}}(T)/T^2 = c_0 \approx 0.075(3) K^{-2}$. Assuming a smooth behavior at low temperature no extra-entropy is expected to be found in this regime. We now fit the part of the experimental data where the phonons are expected to be negligible, that is for $T < 4K$ which includes the peak of $c_V(T)/T$.

Similarly to the magnetic susceptibility (Eq.3), the HT-series expansion of the spin specific heat reads:

$$c_V^{\text{spin}}(T) = \sum_{i=2}^n \frac{q_i(\nu_2, \nu_3)}{i!} \left(\frac{J_1}{2T} \right)^i \quad (12)$$

where q_i are polynomials of order i (see Appendix A).

For two dimensional spin hamiltonians, the function $s(e)$ is more suitable than $c_V(T)$, where s and e are the entropy and energy per spin⁶. Indeed, using sum rules, $s(e)$ is constrained to start at the ground-state energy e_0 with an entropy $s = 0$ and end at $e = 0$ and $s = \ln 2$, at infinite temperature. Moreover this is a monotonic increasing function, $\beta = 1/T = s'(e)$, with negative curvature, $c_V = -s'(e)^2/s''(e)$. Imposing the low temperature power law for $c_V(T)_{T \rightarrow 0} \propto (T/T_0)^\alpha$ implies $s(e)_{e \rightarrow e_0} \propto (e - e_0)^{1/\mu}$, with $\mu = 1 + 1/\alpha$, where here $\alpha = 2$. Thus the function $G(e) = s(e)^\mu/(e - e_0)$ is analytic in the interval $[e_0, 0]$. From the HT-series expansion of $c_V^{\text{spin}}(T)$ we deduce the HT-series expansion of $G(e)$ around $e = 0$ as explained in Appendix D.

The HT-series expansion of $G(e)$ is converted into padé approximant, noted $G_d(e)$ (d being the degree of the denominator), and only *physical* ones (PPA), noted $G_{d^*}(e)$, are kept, i.e. those with no zero in the numerator and denominator in the interval $[e_0, 0]$. It is sufficient to look at $G_{d^*}(e_0)$ to compare different PPAs⁸: indeed all pades have the same series around $e = 0$ and if they have the same value at e_0 it is likely that their variations will be very similar. For anti-ferromagnetic ground states, e_0 is usually unknown. Thus this parameter is determined by maximizing:

$$Q_e(e_0) = \sum_{d_1^*} \sum_{d_2^* > d_1^*} \frac{1}{1 + \left| \frac{G_{d_1^*}(e_0) - G_{d_2^*}(e_0)}{\epsilon_0} \right|^r} \quad (13)$$

where $\epsilon_0 = 10^{-3}$ is of the order of the dispersion $G_{d^*}(e_0)$ in the group of close values and $r = 8$. Note that the found value of e_0 depends only on the HT-series and is thus independent of the fit procedure. Unfortunately, this function may be discontinuous because the number of PPAs may change eventually. Then the maximum of $Q_e(e_0)$ is found after a systematic search on a grid (see Fig.7).

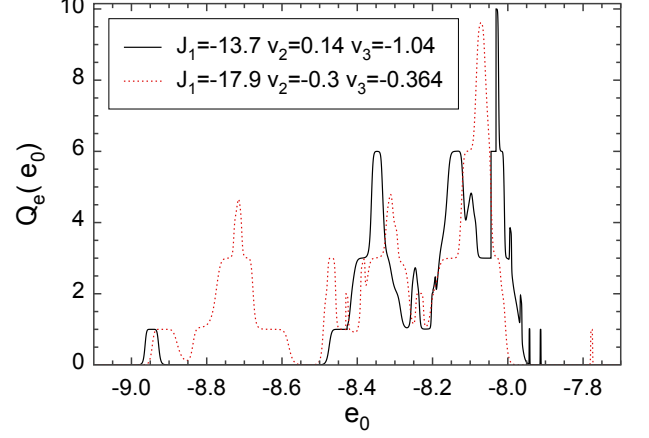


FIG. 7. Variation of Q_e versus the ground state energy e_0 for the two sets of parameters determined in the previous section. Despite the complicated variations, one clear maximum emerges in each case. The number of points in the interval $[-9.1, -7.7]$ is 1000, while the figure is unchanged with ten times more points.

For a fixed set of parameters, once the PPAs of $G(e)$ and e_0 are determined, the spin specific heat are calculated for each PPA, noted $c_{V,PPA}^{\text{spin}}$, as described in Appendix D (Eqs.D8-D10). To compare with experimental data we keep only the data at $T < 4K$ such that the phonon contributions can be neglected. The exchange parameters are determined by maximizing the quality factor Q_{C_V} as follow:

$$Q_{C_V} = \sum_{PPA} \frac{1}{1 + |R_{C_V,PPA}/\epsilon|^r} \quad (14)$$

$$Z_{C_V,PPA} = \sum_{T_k < T_{\text{max}}} \left[D \frac{c_{V,PPA}^{\text{spin}}(T_k)}{T_k} - \frac{c_V^{\text{exp}}(T_k)}{T_k} \right]^2 \quad (15)$$

$$R_{C_V,PPA} = \sqrt{Z_{C_V,PPA}/N_T} \quad (16)$$

where N_T is the number of experimental points with T_k less than T_{max} and we used here $\epsilon = 2 \times 10^{-3}$ and the parameter D , accounting for both mass uncertainty and possible missing entropy, is evaluated as explained in Appendix C.

For the $\{J_1, \nu_2, 0\}$ and $\{J_1, 0, \nu_3\}$ models, no good fit can be found for the specific heat around the domains found for the magnetic susceptibility (see Fig.2).

Computing Q_{C_V} when the e_0 is unknown is much more demanding and less stable and the figures $Q_{C_V}(J_1, \nu_2, \nu_3)$ present lots of discontinuities. Thus proceeding as in the previous section is hopeless. Therefore, we focus of the constrained domain of parameters obtained from the \mathcal{X} analysis (Fig.3). At fixed J_1 and ν_2 we look for ν_3 that maximizes $Q_{\mathcal{X}} + Q_{C_V}$. Fig.8 shows that the global best

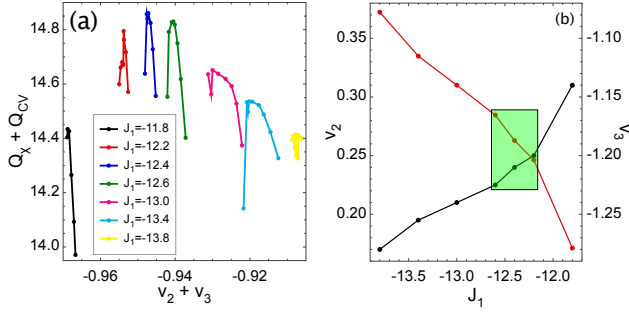


FIG. 8. (a): Optimized values of $Q_X + Q_{CV}$ versus $\nu_2 + \nu_3$ for different values of J_1 . (b): ν_2 and ν_3 versus J_1 for the optimal $Q_X + Q_{CV}$. The green shaded domain indicates the overall optimal values: $J_1 = -12.4(2)$, $\nu_3 = -1.19(3)$, $\nu_2 + \nu_3 = -0.947(7)$.

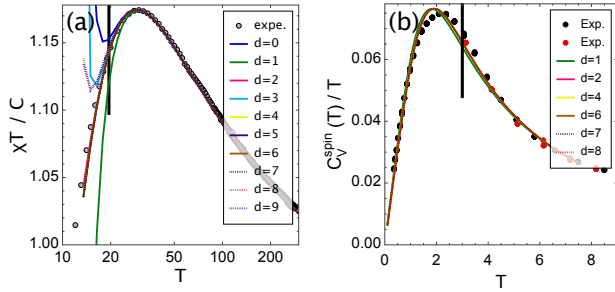


FIG. 9. Comparison with experiments for $J_1 = -12.4$ K, $\nu_2 = 0.24$ and $\nu_3 = -1.1883$. (a): Magnetic susceptibility with $A = 1.028$ and $B = -1.05 \times 10^{-4}$. (b): Specific heat with $D = 0.87$ and $e_0 = -15.53684$ K where PPA- $d = 1$ is slightly different from the others and PPAs- $d = 0$ and $d = 9$ are not shown as being completely off. The vertical line stands for T_{max} (see Eq.15).

fit is obtained for :

$$\begin{aligned}
 J_1 &= -12.4(1) \text{ K} \\
 \nu_3 &= -1.20(4) \\
 \nu_2 + \nu_3 &= -0.95(1) \\
 J_d &= 14.8(8) \text{ K} \\
 J_2 + J_d &= 11.8(4) \text{ K} \\
 J_2 &= -3.1(1.2) \text{ K} \\
 \theta &= 8.1(5) \text{ K} \\
 J_{CV} &= 10.1(4) \text{ K}
 \end{aligned} \tag{17}$$

Fig.9 shows the best overall comparison with experiments at this point.

IV. CONCLUSION

We have fitted the spin contribution of the magnetic susceptibility and specific heat experimental data with a

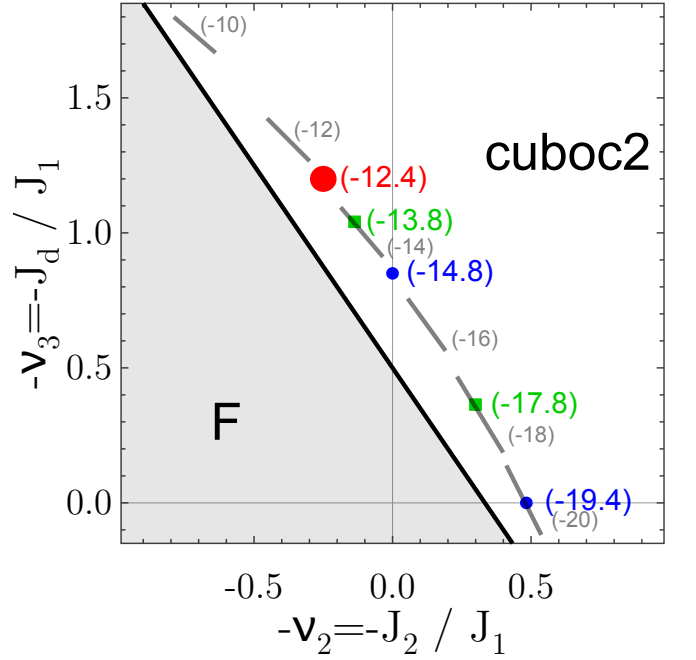


FIG. 10. Optimal parameters of the fits in the J_1 - J_d - J_d classical phase diagram ($J_1 = -1$) of ref.⁹. All fits are in the cuboc2 phase. The blue dots are the estimations of the best two-parameter models. Grey lines represent the narrow domain, at fixed J_1 , where $Q_X > 5$ (Eq.6). The green squares represent the best two values obtained from the fit of the magnetic susceptibility. The red large dot is the best compromise for the magnetic susceptibility and the specific heat. Numbers in parenthesis stand for the corresponding J_1 values.

spin-1/2 J_1 - J_2 - J_d Heisenberg model on the kagome lattice (see Fig.1). In contradiction to ab initio calculations of Janson⁵ the nearest neighbor coupling is ferromagnetic. This is at variance with Herbertsmithite where the nearest neighbor interaction is strong and antiferromagnetic. This can be traced back to the Cu- μ_3 OH-Cu bonding angle being $\sim 13^\circ$ smaller in kapellasite^{2,10}. The related compound Haydeeite $\text{Cu}_3\text{Mg}(\text{OH})_6\text{Cl}_2$, has also a ferromagnetic first neighbor interaction but is in the ferromagnetic domain.^{2,11} This is not the case of kapellasite where the J_2 and J_d exchange couplings compete to form a non magnetic compound.

The spin susceptibility is relatively easy to reproduce and imposes strong correlations of J_1 , J_2 and J_d along a narrow line (see Fig.10). All solutions stay in the antiferromagnetic cuboc2 domain of the classical phase diagram (we do not expect the ferro-cuboc2 transition line to move significantly for spin-1/2 spins)⁹. The main distinctive features of the specific heat data are the low- T downturn in C_v/T at about 2K, characteristic of the competitive exchange couplings and a clear T^2 dependency excluding a ferromagnetic ground state. The peak strongly constrains the parameters. The best domain

for both the magnetic susceptibility and the specific heat corresponds to J_1 between -12 and -14 K, J_2 small and ferromagnetic and a large anti-ferromagnetic J_d (see red dot in Fig.10). Thus competitive exchange energies give here a ferromagnetic behavior of the magnetic susceptibility at high temperature but an anti-ferromagnetic one at low temperature for specific heat.

However the agreement between experiment and theory is not as good as a quick glance on Fig. 9 would suggest. There is about 10% of missing entropy ($D = 0.87$ in Eq.15 whereas the mass uncertainties is of only about a few percent) in our description. Considering improbable to find this missing entropy at very low temperature, we have to find it at intermediate temperature between 2 and 20 K where we have not succeeded to fit the full specific heat variations with this spin model and phonon contributions. Indeed Kapellasite has about 27% missing spins (Cu atoms replaced by Zn ones) on the kagome sites and also a few percent of Cu atoms at the center of the hexagons. This concentration of Zn on the kagome sites is not enough to kill the cuboc2 correlations, the threshold being at about 40%¹². But triangles with a Zn substitution (about 42%) may favor the formation of singlets and thus freeze entropy at low temperature. (The spins at the center of the hexagons in a symmetric environment experience a magnetic field at second order in perturbation and are probably only weakly coupled to their neighbors.) The quantum description of such a phenomenon is for the moment out of the possibilities of any approach and theoreticians have to wait for the synthesis of compounds with less defects. On the other hand, taking into account these two types of defects would probably allow to fit the magnetic susceptibility to lower temperatures. (Indeed, the pade approximants of the susceptibility converge to lower temperature than $T_{\min} \sim 20K$, the temperature where the pades and the experimental χ data points do not agree anymore.)

A last limit on this determination is the neglect of Dzyaloshinskii-Moriya interactions. In fact the lack of inversion center on the magnetic bounds allows for Dzyaloshinskii-Moriya interaction of spin orbit origin. In the cuprates in general these couplings are estimated of the order of 1/10 of the super exchange couplings and in Herbersmithite they were measured of the order of $0.06(2)K$ ¹³. It is well known that the influence of this small coupling is of crucial importance in Herbersmithite^{14,15}, in which it very plausibly explains the critical behavior of the compound^{16,17,19}. But in that case the influence of this tiny coupling is indeed emphasized by the fact that the anti-ferromagnetic Heisenberg hamiltonian is classically at a multi-critical point and quantum mechanically nearby a quantum critical point.¹⁶ The situation in Kapellasite is quite different: whereas neutron scattering in Herbersmithite is essentially featureless¹⁸⁻²⁰ the experimental evidence of short range cuboc2 correlations in Kapellasite is strong³, and the results of the present analysis (see Fig.10) point in the same direction: the J_2 and J_d parameters are not fitted

unambiguously but all the fits agree to locate the system in the cuboc2 range, very far away from any critical point (the cuboc2-ferro transition is a strong first order transition²¹). Extending the present fit to take into account Dzyaloshinskii-Moriya interactions would slightly change the exchange parameters but not move the system away from the present phase. With these caveats in mind, we think that the present model is the best effective model that we are able to build.

Appendix A: HT-series expansion

We give here the susceptibility HT-series polynomials as defined by Eq.3:

$$p_0(\nu_2, \nu_3) = 1 \quad (\text{A1})$$

$$p_1(\nu_2, \nu_3) = -2 - 2\nu_2 - \nu_3 \quad (\text{A2})$$

$$p_2(\nu_2, \nu_3) = 4 + 8\nu_3 + 16\nu_2 + 8\nu_2\nu_3 + 4\nu_2^2 \quad (\text{A3})$$

$$p_3(\nu_2, \nu_3) = -3 - 48\nu_3 - 81\nu_2 - 3\nu_2^3 - 48\nu_2^2\nu_3 + 2\nu_3^3 - 12\nu_2\nu_3^2 - 114\nu_2\nu_3 - 96\nu_2^2 - 12\nu_2^2 \quad (\text{A4})$$

$$p_4(\nu_2, \nu_3) = -4 + 176\nu_3 + 172\nu_2 - 4\nu_2^4 - 32\nu_2\nu_3^3 + 216\nu_2^3\nu_3 + 5\nu_3^4 + 260\nu_2^2\nu_3^2 + 396\nu_2\nu_3^2 + 1188\nu_2^2\nu_3 + 432\nu_2^3 - 32\nu_3^3 + 1094\nu_2^2 + 1108\nu_2\nu_3 + 260\nu_2^2 \quad (\text{A5})$$

$$p_5(\nu_2, \nu_3) = -202 + 225\nu_3 + 605\nu_2 - 680\nu_2^4\nu_3 - 202\nu_2^5 - 21\nu_3^5 - 270\nu_2^2\nu_3^3 + 60\nu_2\nu_3^4 - 3245\nu_2^3\nu_3^2 - 11430\nu_2^2\nu_3^3 + 60\nu_3^4 - 7970\nu_2^2\nu_3^2 - 410\nu_2\nu_3^3 - 1360\nu_2^4 - 270\nu_3^3 - 8465\nu_2\nu_3^2 - 17230\nu_2^2\nu_3 - 11645\nu_2^3 - 2935\nu_3^2 - 7630\nu_2\nu_3 - 5595\nu_2^2 \quad (\text{A6})$$

$$p_6(\nu_2, \nu_3) = 1513 + 4104\nu_2 - 4206\nu_3 - 14253\nu_2^2 + 122658\nu_2\nu_3^2 + 187998\nu_2^2\nu_3 + 15912\nu_2\nu_3 + 132562\nu_2^3 + 13170\nu_3^2 + 20210\nu_3^3 + 98088\nu_2^4 + 251238\nu_2^3\nu_3 + 40632\nu_2\nu_3^3 + 183249\nu_2^2\nu_3^2 - 2646\nu_2\nu_3^4 + 104100\nu_2^4\nu_3 + 132630\nu_2^3\nu_3^2 + 38550\nu_2^2\nu_3^3 - 4170\nu_2^2\nu_3^4 + 18080\nu_2^3\nu_3^3 + 26370\nu_2^4\nu_3^2 + 3384\nu_2^5\nu_3 + 1104\nu_2\nu_3^5 - 4170\nu_3^4 + 1104\nu_3^5 + 6768\nu_2^5 + 1513\nu_2^6 - \frac{399}{2}\nu_3^6 \quad (\text{A7})$$

$$p_7(\nu_2, \nu_3) = 13844 - 151620\nu_2 - 74704\nu_3 + 139083\nu_2^2 - \frac{1966153}{2}\nu_2\nu_3^2 - 1293383\nu_2^2\nu_3 + 299964\nu_2\nu_3 - \frac{189371}{2}\nu_2^3 + 139755\nu_3^2 - 371574\nu_3^3 - \frac{4759391}{2}\nu_2^4 - 3589292\nu_2^3\nu_3 - 1154895\nu_2^2\nu_3^2 - \frac{6770421}{2}\nu_2^2\nu_3^2 - \frac{82789}{2}\nu_2\nu_3^4 - 3827614\nu_2^4\nu_3 - 3512439\nu_2^3\nu_3^2 - 1749132\nu_2^2\nu_3^3 - 86618\nu_2^2\nu_3^4 - 990822\nu_2^3\nu_3^3 - 1991059\nu_2^4\nu_3^2 - 775061\nu_2^5\nu_3 + 7651\nu_2\nu_3^5 - 354109\nu_2^4\nu_3^3 + 938\nu_2\nu_3^6 + \frac{67319}{2}\nu_2^3\nu_3^4 - 53018\nu_2^6\nu_3 - 3738\nu_2^2\nu_3^5 - \frac{262773}{2}\nu_2^5\nu_3^2 + 13615\nu_3^4 - 3738\nu_3^5 - \frac{1275309}{2}\nu_2^5 - 106036\nu_2^6 + 938\nu_3^6 + 13844\nu_2^7 + 160\nu_3^7 \quad (\text{A8})$$

$$p_8(\nu_2, \nu_3) = -186286 - 137536\nu_2 + 1145568\nu_3 + 6324260\nu_2^2 - 2088608\nu_2\nu_3^2 - 4756328\nu_2^2\nu_3 + 857352\nu_2\nu_3 - 10846320\nu_3^2 - 1664724\nu_2^3 + 1483992\nu_3^3 + 16142374\nu_2^4 + 41699268\nu_2^3\nu_3 + 19842784\nu_2\nu_3^3 + 40719726\nu_2^2\nu_3^2$$

$$+ 6650764\nu_2\nu_3^4 + 67176864\nu_2^4\nu_3 + 82220052\nu_2^3\nu_3^2 + 42915800\nu_2^2\nu_3^3 + 10425242\nu_2^2\nu_3^4 + 46137688\nu_2^3\nu_3^3 + 65417170\nu_2^4\nu_3^2 + 54159980\nu_2^5\nu_3 - 1232896\nu_2\nu_3^5 + 18554568\nu_2^4\nu_3^3 + 127572\nu_2\nu_3^6 + 6383884\nu_2^3\nu_3^4 + 3657208\nu_2^6\nu_3 - 1281328\nu_2^2\nu_3^5 + 26510312\nu_2^5\nu_3^2 + 2892272\nu_3^4 - 870832\nu_3^5 + 32058256\nu_2^5 + 4069692\nu_2^6 + 248420\nu_3^6 + 764352\nu_2^7 - 61008\nu_3^7 - 186286\nu_2^8 + 11421\nu_3^8 + 248420\nu_2^2\nu_3^6 - 592716\nu_2^3\nu_3^5 + 1625812\nu_2^4\nu_3^4 + 4060012\nu_2^5\nu_3^3 + 811044\nu_2^6\nu_3^2 - 61008\nu_2\nu_3^7 + 382176\nu_2^7\nu_3 \quad (\text{A9})$$

$$p_9(\nu_2, \nu_3) = -2329677 + 26960814\nu_2 + 11526543\nu_3 - 56758545\nu_2^2 + 128462472\nu_2\nu_3^2 + 154668708\nu_2^2\nu_3 - 111054150\nu_2\nu_3 - 115342752\nu_2^3 - 36200385\nu_3^2 + 64998198\nu_3^3 + 319743243\nu_2^4 - 220814460\nu_2^3\nu_3 - 147995460\nu_2\nu_3^3 - 152834616\nu_2^2\nu_3^2 - 244445922\nu_2\nu_3^4 - 822646359\nu_2^4\nu_3 - 1365041772\nu_2^3\nu_3^2 - 706484844\nu_2^2\nu_3^3 - 436794300\nu_2^2\nu_3^4 - 1401175632\nu_2^3\nu_3^3 - 1793770353\nu_2^4\nu_3^2 - 1427828508\nu_2^5\nu_3 + 3083328\nu_2\nu_3^5 - 944463996\nu_2^4\nu_3^3 + 2878929\nu_2\nu_3^6 - 456663087\nu_2^3\nu_3^4 - 576786222\nu_2^6\nu_3 + 24409008\nu_2^5\nu_3^2 - 1226646711\nu_2^5\nu_3^2 - 81429093\nu_3^4 + 14618331\nu_3^5 - 580389138\nu_2^5 - 314815344\nu_2^6 - 3893763\nu_3^6 - 55709883\nu_2^7 + 1180962\nu_3^7 + 7338168\nu_2^8 - 311904\nu_3^8 + 7769322\nu_2^2\nu_3^6 - 13919346\nu_2^3\nu_3^5 - 172316772\nu_2^4\nu_3^4 - 380586006\nu_2^5\nu_3^3 - 287537220\nu_2^6\nu_3^2 - 965718\nu_2\nu_3^7 - 27272862\nu_2^7\nu_3 + 1180962\nu_2^2\nu_3^7 - 5141667\nu_2^3\nu_3^6 + 9044406\nu_2^4\nu_3^5 - 59040405\nu_2^5\nu_3^4 - 33586860\nu_2^6\nu_3^3 - 20688669\nu_2^7\nu_3^2 - 311904\nu_2\nu_3^8 + 3669084\nu_2^8\nu_3 - 2329677\nu_2^9 + 37370\nu_3^9 \quad (\text{A10})$$

$$p_{10}(\nu_2, 0) = 44494564 + 32699900\nu_2 - 1607336300\nu_2^2 + 4682885400\nu_2^3 - 1969984450\nu_2^4 - 3722864284\nu_2^5 + 12819641560\nu_2^6 + 2641862210\nu_2^7 + 853326455\nu_2^8 - 109501560\nu_2^9 + 44494564\nu_2^{10} \quad (\text{A11})$$

$$p_{10}(0, \nu_3) = 44494564 - 323940580\nu_3 + 753910650\nu_3^2 - 746061580\nu_3^3 + 248953155\nu_3^4 + 673343648\nu_3^5 - 251041900\nu_3^6 + 86401210\nu_3^7 - 21228160\nu_3^8 + 4486600\nu_3^9 - \frac{1698455}{2}\nu_3^{10} \quad (\text{A12})$$

$$p_{11}(0, \nu_3) = 568071766 - \frac{5959595279}{2}\nu_3 + \frac{19215984161}{2}\nu_3^2 - \frac{49178193933}{2}\nu_3^3 + 33878328495\nu_3^4 - 30148742943\nu_3^5 + 8479066530\nu_3^6 - 2914976526\nu_3^7 + \frac{1749626615}{2}\nu_3^8 - 246955709\nu_3^9 + 58891206\nu_3^{10} - 8569254\nu_3^{11} \quad (\text{A13})$$

We give here the specific heat HT-series polynomials as defined by Eq.12:

$$q_0(\nu_3, \nu_3) = 0 \quad (\text{A14})$$

$$q_1(\nu_3, \nu_3) = 0 \quad (\text{A15})$$

$$q_2(\nu_3, \nu_3) = 3 + 3\nu_2^2 + \frac{3}{2}\nu_3^2 \quad (\text{A16})$$

$$q_3(\nu_3, \nu_3) = -27\nu_2 - 54\nu_3\nu_2 + \frac{9}{2}\nu_3^3 \quad (\text{A17})$$

$$q_4(\nu_3, \nu_3) = -153 + 144\nu_2 + 108\nu_3 + 144\nu_3\nu_2 - 90\nu_3^2 \\ + 252\nu_3\nu_2^2 - 72\nu_3^2\nu_2 - 153\nu_2^4 - 90\nu_3^2\nu_2^2 - \frac{45}{2}\nu_3^4 \quad (\text{A18})$$

$$q_5(\nu_3, \nu_3) = 3300\nu_2 - 900\nu_3 - 2850\nu_2^2 + 5700\nu_3\nu_2 \\ - 150\nu_3^2 + 1650\nu_3^2 - 4650\nu_3\nu_2^2 + 750\nu_3^2\nu_2 - 450\nu_3^3 \\ + 6000\nu_3\nu_2^3 - 1350\nu_3^2\nu_2^2 + 3300\nu_3^3\nu_2 - 300\nu_3^2\nu_2^3 \\ - 450\nu_3^3\nu_2^2 - 225\nu_3^5 \quad (\text{A19})$$

$$q_6(\nu_3, \nu_3) = 32085/2 - 24570\nu_2 - 20655\nu_3 - 21735\nu_2^2 \\ + 1620\nu_3\nu_2 + \frac{33615}{2}\nu_3^2 + 19890\nu_2^3 - 131085\nu_3\nu_2^2 \\ + 43200\nu_3^2\nu_2 - 9225\nu_3^3 + 9450\nu_2^4 + 46980\nu_3\nu_2^3 \\ - 81675\nu_3^2\nu_2^2 - 2430\nu_3^3\nu_2 + \frac{8235}{2}\nu_3^4 - 32805\nu_3\nu_2^4 \\ + 54000\nu_3^2\nu_2^3 - 28080\nu_3^3\nu_2^2 + 19710\nu_3^4\nu_2 + \frac{32085}{2}\nu_2^6 \\ + 16875\nu_3^2\nu_2^4 + 4950\nu_3^3\nu_2^3 + \frac{8235}{2}\nu_3^4\nu_2^2 + \frac{945}{4}\nu_3^6 \quad (\text{A20})$$

$$q_7(\nu_3, \nu_3) = -10143 - 644301\nu_2 + 269892\nu_3 + 1052226\nu_2^2 \\ - 934920\nu_3\nu_2 - 75411\nu_3^2 - 460404\nu_2^3 + 1893654\nu_3\nu_2^2 \\ - 31752\nu_3^2\nu_2 + 122598\nu_3^3 + 119511\nu_2^4 - 1000629\nu_3\nu_2^3 \\ + 242991\nu_3^2\nu_2^2 - 1032381\nu_3^3\nu_2 - 31311\nu_3^4 - \frac{930069}{2}\nu_2^5 \\ + 269010\nu_3\nu_2^4 + 827757\nu_3^2\nu_2^3 - 257544\nu_3^3\nu_2^2 \\ - \frac{125685}{2}\nu_3^4\nu_2 + 58653\nu_3^5 - 1421343\nu_3\nu_2^5 \\ - 187425\nu_3^2\nu_2^4 - 980343\nu_3^3\nu_2^3 + \frac{52479}{2}\nu_3^4\nu_2^2 \\ - 227997\nu_3^5\nu_2 - 10143\nu_2^7 + 7938\nu_3^2\nu_2^5 - 38808\nu_3^3\nu_2^4 \\ + 66150\nu_3^4\nu_2^3 + 58653\nu_3^5\nu_2^2 + \frac{57771}{4}\nu_3^7 \quad (\text{A21})$$

$$q_8(\nu_3, \nu_3) = -2859213 + 6178704\nu_2 + 5449416\nu_3 \\ + 9429168\nu_2^2 - 9235296\nu_3\nu_2 - 4847052\nu_3^2 \\ - 20274912\nu_2^3 + 53705904\nu_3\nu_2^2 - 21687792\nu_3^2\nu_2 \\ + 5012952\nu_3^3 + 9225132\nu_2^4 - 62253744\nu_3\nu_2^3 \\ + 48280344\nu_3^2\nu_2^2 + 3022992\nu_3^3\nu_2 - 1229970\nu_3^4 \\ - 1534176\nu_2^5 + 56331912\nu_3\nu_2^4 - 65766624\nu_3^2\nu_2^3 \\ + 40230624\nu_3^3\nu_2^2 - 12512304\nu_3^4\nu_2 + 1025136\nu_3^5$$

$$- 626304\nu_2^6 - 7418544\nu_3\nu_2^5 + 43961232\nu_3^2\nu_2^4 \\ - 8318688\nu_3^3\nu_2^3 + 23324616\nu_3^4\nu_2^2 - 130368\nu_3^5\nu_2 \\ - 125076\nu_3^6 + 10753344\nu_3\nu_2^6 - 12882912\nu_3^2\nu_2^5 \\ + 10512768\nu_3^3\nu_2^4 - 13091568\nu_3^4\nu_2^3 + 4212600\nu_3^5\nu_2^2 \\ - 3452400\nu_3^6\nu_2 - 2859213\nu_2^8 - 3844932\nu_3^2\nu_2^6 \\ - 741888\nu_3^3\nu_2^5 - 2292990\nu_3^4\nu_2^4 - 654192\nu_3^5\nu_2^3 \\ - 125076\nu_3^6\nu_2^2 + \frac{89271}{2}\nu_3^8 \quad (\text{A22})$$

$$q_9(\nu_3, \nu_3) = 5600664 + 184435056\nu_2 - 100067400\nu_3 \\ - 433650996\nu_2^2 + 227967048\nu_3\nu_2 + 78952644\nu_3^2 \\ + 179433792\nu_2^3 - 607203540\nu_3\nu_2^2 - 42816600\nu_3^2\nu_2 \\ - 63694188\nu_3^3 + 95703120\nu_2^4 - 144709416\nu_3\nu_2^3 \\ + 485374032\nu_3^2\nu_2^2 + 276310440\nu_3^3\nu_2 + 35501328\nu_3^4 \\ + 123924168\nu_2^5 + 441623340\nu_3\nu_2^4 - 1670214816\nu_3^2\nu_2^3 \\ + 372083544\nu_3^3\nu_2^2 - 127644984\nu_3^4\nu_2 - 24001596\nu_3^5 \\ - 70144056\nu_2^6 + 144516960\nu_3\nu_2^5 + 1235200104\nu_3^2\nu_2^4 \\ - 631218096\nu_3^3\nu_2^3 + 54034452\nu_3^4\nu_2^2 + 115234488\nu_3^5\nu_2 \\ + 10998828\nu_3^6 + 146195604\nu_2^7 - 127553616\nu_3\nu_2^6 \\ - 684430884\nu_3^2\nu_2^5 + 852307920\nu_3^3\nu_2^4 - 593753004\nu_3^4\nu_2^3 \\ + 250454268\nu_3^5\nu_2^2 + 4221396\nu_3^6\nu_2 - 8027748\nu_3^7 \\ + 442063656\nu_3\nu_2^7 + 75600216\nu_3^2\nu_2^6 + 423090216\nu_3^3\nu_2^5 \\ + 106291116\nu_3^4\nu_2^4 + 101241576\nu_3^5\nu_2^3 + 22410432\nu_3^6\nu_2^2 \\ + 12159720\nu_3^7\nu_2 + 5600664\nu_2^9 + 4667544\nu_3^2\nu_2^7 \\ + 32428512\nu_3^3\nu_2^6 - 21895272\nu_3^4\nu_2^5 + 2416392\nu_3^5\nu_2^4 \\ - 17600328\nu_3^6\nu_2^3 - 8027748\nu_3^7\nu_2^2 - 1161810\nu_3^9 \quad (\text{A23})$$

$$q_{10}(\nu_2, 0) = \frac{559095695}{2} - 2276071650\nu_2 - 4567367250\nu_2^2 \\ + 14999658300\nu_2^3 - 11395200825\nu_2^4 + 3512454300\nu_2^5 \\ - 4851077175\nu_2^6 + 1271847150\nu_2^7 - 191251800\nu_2^8 \\ + \frac{1559095695}{2}\nu_2^{10} \quad (\text{A24})$$

$$q_{10}(0, \nu_3) = \frac{559095695}{2} - 1968883875\nu_3 + \frac{3707972775}{2}\nu_3^2 \\ - 2766779100\nu_3^3 + 953949150\nu_3^4 - 929445975\nu_3^5 \\ + 73620225\nu_3^6 - 111223125\nu_3^7 - \frac{59072625}{2}\nu_3^8 \\ - \frac{45148455}{4}\nu_3^{10} \quad (\text{A25})$$

$$q_{11}(0, \nu_3) = 3188690010 + 49046431005\nu_3 \\ - \frac{127470667995}{2}\nu_3^2 + \frac{103764854985}{2}\nu_3^3 \\ - 41081190975\nu_3^4 + 16829360625\nu_3^5 - 15771729270\nu_3^6 \\ + \frac{10254468675}{2}\nu_3^7 - 3039511530\nu_3^8 + 1205526630\nu_3^9 \\ + \frac{390259485}{4}\nu_3^{11} \quad (\text{A26})$$

Appendix B: Physical Pade Approximant (PPA)

For fixed values of the coupling constants J_1 , J_2 and J_d , we evaluate the order- n HT-polynomial of the magnetic susceptibility, $\chi_n^{\text{HT}}(\beta)$, or of the specific heat, $C_{V,n}^{\text{spin,HT}}(e)$, where e is the energy per spin. From a polynomial $f_n(x)$ of order n we calculate $n+1$ rational fractions $p_{n-d}(x)/q_d(x)$ with d running from 0 to n . A PPA must have no zero in p and q in the whole interval of variation of x , i.e. in $[0, \infty]$ for $\chi_n^{\text{HT}}(\beta)$ and $[e_0, 0]$ for $C_{V,n}^{\text{spin,HT}}(e)$, where e_0 is the ground state energy. Solutions with zero in the range of interest are discarded. By varying the coupling parameters, the number of PPAs may eventually change. Thus all functions build on the sum over the PPAs are discontinuous. Unfortunately this prevents from using minimization powerful method. This is a price to pay when using PPAs.

Appendix C: Determination of the parameters A and B of Q_X

From Eq.6 or Eq.14, we have:

$$Q_X = \sum_{PPA} \frac{1}{1 + |R_{X,PPA}/\epsilon|^r} \quad (\text{C1})$$

$$R_{X,PPA} = \sum_k [AF_{PPA}(T_k) + BT_k - F_k^{\text{exp}}]^2 \quad (\text{C2})$$

where $X = \mathcal{X}$ or C_V and B is 0 for C_V .

$$\begin{aligned} \frac{\partial Q_X}{\partial A} &= - \sum_{\{PPA\}} \frac{\partial Q_{X,PPA}}{\partial A} \\ &= - \frac{r}{2\epsilon^2 N_T} \sum_{\{PPA\}} \frac{Q_{X,PPA}^{1+2/r}}{(1 - Q_{X,PPA})^{1-2/r}} \\ &\quad \times \sum_{k=1}^{N_T} [(AF_{PPA}(T_k) - BT_k - F_k^{\text{exp}}) F_{PPA}(T_k)] \end{aligned} \quad (\text{C3})$$

$$\begin{aligned} \frac{\partial Q_X}{\partial B} &= - \frac{r}{2\epsilon^2 N_T} \sum_{\{PPA\}} \frac{Q_{X,PPA}^{1+2/r}}{(1 - Q_{X,PPA})^{1-2/r}} \\ &\quad \times \sum_{k=1}^{N_T} [(AF_{PPA}(T_k) - BT_k - F_k^{\text{exp}}) T_k] \end{aligned} \quad (\text{C4})$$

where F stands for $\mathcal{X}T/C$ or C_V/T . We look for A and B that cancel out these derivatives. First, A and B are evaluated for each PPA:

$$A_{PPA} = \frac{1}{\Delta} \left(\overline{T F^{\text{exp}}} \overline{T F_{PPA}} - \overline{T^2} \overline{F_{PPA} F^{\text{exp}}} \right) \quad (\text{C5})$$

$$B_{PPA} = \frac{1}{\Delta} \left(\overline{F_{PPA} T} \overline{F_{PPA} F^{\text{exp}}} - \overline{T F^{\text{exp}}} \overline{F_{PPA}^2} \right) \quad (\text{C6})$$

$$\Delta = \overline{T F_{PPA}^2} - \overline{T^2} \overline{F_{PPA}^2} \quad (\text{C7})$$

where \overline{X} means the average value over the set of temperatures. Then, the best PPA (highest $Q_{X,PPA}$) leads to the first values (A_{PPA} , B_{PPA}) which are used to compute the $Q_{X,PPA}$ and Eqs.C3-C4 are solved as:

$$A = \frac{1}{\Delta} \left(\langle \overline{T F^{\text{exp}}} \rangle \langle \overline{T F_{PPA}} \rangle - \langle \overline{T^2} \rangle \langle \overline{F_{PPA} F^{\text{exp}}} \rangle \right) \quad (\text{C8})$$

$$B = \frac{1}{\Delta} \left(\langle \overline{F_{PPA} T} \rangle \langle \overline{F_{PPA} F^{\text{exp}}} \rangle - \langle \overline{T F^{\text{exp}}} \rangle \langle \overline{F_{PPA}^2} \rangle \right) \quad (\text{C9})$$

$$\Delta = \langle \overline{T F_{PPA}^2} \rangle - \langle \overline{T^2} \rangle \langle \overline{F_{PPA}^2} \rangle \quad (\text{C10})$$

where $\langle \overline{X} \rangle$ means the average value over the set of temperatures and over the PPA with the weights $Q_{X,PPA}^{1+2/r}/(1 - Q_{X,PPA})^{1-2/r}$. The procedure is iterated until convergence by calculating the new weights at the new A and B . The convergence is quick and a couple of iterations are sufficient for a relative precision of 10^{-5} on A and B .

Appendix D: Pade approximant for C_V

We first determine the HT-series of $s(e)$ the entropy per spin versus the energy per spin⁶: From the HT-series expansion of $C_V(T) = \sum_{i=2}^n a_i \beta^i$, with $\beta = 1/T$, we obtain the HT-series of $s(T)$ and $e(T)$ as:

$$\begin{aligned} s(T) &= \ln 2 - \int_T^\infty dT' \frac{C_V^{\text{spin}}(T')}{T'} \\ &= \ln 2 - \sum_{i=2}^n \frac{a_i}{i} \beta^i + \mathcal{O}(\beta^{n+1}) \end{aligned} \quad (\text{D1})$$

$$\begin{aligned} e(T) &= - \int_T^\infty dT' C_V^{\text{spin}}(T') \\ &= - \sum_{i=2}^{n-1} \frac{a_{i+1}}{i} \beta^i + \mathcal{O}(\beta^n) \end{aligned} \quad (\text{D2})$$

where we use $s(T = \infty) = \ln 2$ and $e(T = \infty) = 0$. The HT-series expansion of $s(e)$:

$$s(e) = \sum_{i=0}^n b_i e^i \quad (\text{D3})$$

is obtained order by order using (Maple style):

```
for i from 0 to n do
  ss:=0;
  for j from 0 to i-1 do
    ss:=ss+b[j]*coeff(E^j,beta,i);
  od;
  b[i]:=(coeff(S,beta,i)-ss)/coeff(E^i,beta,i);
od;
```

where S and E stand for the HT-series of $s(T)$ and $e(T)$.

The low- T leading term of $C_V(T)$ is assumed to be $(T/T_0)^\alpha$. Then $s(e) \propto (e - e_0)^{1/\mu}$ for e around e_0 where e_0 is the ground state energy and $\mu = 1 + 1/\alpha$. We define a function:

$$G(e) = \frac{s(e)^\mu}{e - e_0}. \quad (\text{D4})$$

The HT-series expansion for $G(e)$ is obtained from:

$$G(e) = -\frac{(\ln 2)^\mu}{e_0} \left[\sum_{i=0}^n F_i(\mu) \frac{P(e)^i}{i!} \right] \left[\sum_{i=0}^n (e/e_0)^i \right] \quad (\text{D5})$$

$$P(e) = \frac{s(e)}{\ln 2} - 1 = \sum_{i=2}^n \tilde{b}_i e^i \quad (\text{D6})$$

where $\tilde{b}_i = b_i / \ln 2$ ($b_1 = 0$) and $F_i(\mu) = \Gamma(\mu + 1) / \Gamma(\mu + 1 - i) = \mu(\mu - 1) \dots (\mu + 1 - i)$. Keeping only terms up to order n defines $G^{\text{HT}}(e)$. Note that $P(e)^i$ starts at order $2i$.

Then $G^{\text{HT}}(e)$ is transformed in all possible pade approximants noted $G_{d^*}^{\text{HT}}(e)$ where $n - d$ and d are the numerator and denominator degrees. We keep only

the *physical* pade approximants (PPA) denoted $G_{d^*}^{\text{HT}}(e)$ whose numerator or denominator have no zero inside the $[e_0, 0]$. The value $G_{d^*}^{\text{HT}}(e_0)$ is related to c_0 (see Eq.11):

$$G_{d^*}^{\text{HT}}(e_0) = c_{0,d^*}^{\mu-1} \frac{\alpha + 1}{\alpha^\mu} \quad (\text{D7})$$

From a $G_{d^*}^{\text{HT}} = N_{n-d^*}(e) / D_{d^*}(e)$, we obtain first $s(e)$ and its first derivatives and then the specific heat:

$$s_{d^*}(e) = \left[(e - e_0) \frac{N(e)}{D(e)} \right]^{1/\mu} \quad (\text{D8})$$

$$\mu \frac{s'_{d^*}(e)}{s_{d^*}(e)} = \frac{1}{e - e_0} + \frac{N'(e)}{N(e)} - \frac{D'(e)}{D(e)} \quad (\text{D9})$$

$$\begin{aligned} \mu \frac{s''_{d^*}(e)}{s_{d^*}(e)} = & \mu \left[\frac{s'_{d^*}(e)}{s_{d^*}(e)} \right]^2 + \frac{N''(e)}{N(e)} - \frac{D''(e)}{D(e)} \\ & - \left[\frac{N'(e)}{N(e)} \right]^2 + \left[\frac{D'(e)}{D(e)} \right]^2 - \frac{1}{(e - e_0)^2} \end{aligned} \quad (\text{D10})$$

Then we deduce $\beta(e) = 1/T(e) = s'_{d^*}(e)$ and $c_V^{\text{spin}}(e) = -[s'_{d^*}(e)]^2 / s''_{d^*}(e)$.

-
- ¹ R. H. Colman, C. Ritter, and A. S. Wills, Chem. Mater. **20**, 6897 (2008).
 - ² R. H. Colman, A. Sinclair, and A. S. Wills, Chem. Mater. **22**, 5774 (2010).
 - ³ B. Fåk, E. Kermarrec, L. Messio, B. Bernu, C. Lhuillier, F. Bert, P. Mendels, B. Koteswararao, F. Bouquet, J. Ollivier, A. D. Hillier, A. Amato, R. H. Colman, and A. S. Wills, Phys. Rev. Lett., 109, 037208 (2012).
 - ⁴ D.S. Greywall and P.A. Busch, Phys. Rev. Lett. **65** 2788 (1990); D.S. Greywall Phys. Rev. B **41** 1842 (1990);
 - ⁵ O. Janson, J. Richter, and H. Rosner, Phys. Rev. Lett. **101**, 106403 (2008).
 - ⁶ B. Bernu, G. Misguich. cond-mat/0003381, Phys. Rev. B. **63**, p.134409 (2001).
 - ⁷ F. Bert, S. Nakamae, F. Ladieu, D. LHte, P. Bonville, F. Duc, J.-C. Trombe, and P. Mendels, Phys. Rev. B **76**, 132411 (2007); G. Misguich and P. Sindzingre, Eur. Phys. J. B, **59**, 305 (2007); A. Olariu, P. Mendels, F. Bert, F. Duc, J. C. Trombe, M. A. de Vries, and A. Harrison, Phys. Rev. Lett. **100**, 087202 (2008); P. Mendels and A. Wills, in "Introduction to Frustrated Magnetism", Eds C. Lacroix, P. Mendels and F. Mila, Springer-Verlag (2011)
 - ⁸ G. Misguich, B. Bernu, L. Pierre cond-mat/0302583, Phys. Rev. B. **68**, 113409 (2003)
 - ⁹ L. Messio, C. Lhuillier, and G. Misguich, Phys. Rev. B **83**, 184401 (2011).
 - ¹⁰ A. S. Wills and J.-Y. Henry, J. Phys. Condens. Matter **20**, 472206 (2008).
 - ¹¹ Shaoyan Chu, J. Phys.: Conf. Ser. **273** 012123 (2011). Confirmed by our fit, to be published.
 - ¹² F. Briec, B. Bernu, P. Viot, C.Lhuillier, Classical analysis, To be published.
 - ¹³ A. Zorko, S. Nellutla, J. van Tol, L.C. Brunel, F. Bert, F. Duc, J. C. Trombe, M.A. de Vries, A. Harrison and P. Mendels, Phys. Rev. Lett. **101**, 026405 (2008); El Shawish, S., Cépas, O. and Miyashita, S. Phys. Rev. B **81**, 224421 (2010). Han, Tianheng and Chu, Shaoyan and Lee, Young S., Phys. Rev. Lett., **108**, 157202 (2012)
 - ¹⁴ M. Rigol and R.R. P. Singh, Physical Review Letters, **98** 207204 (2007).
 - ¹⁵ M. Rigol and R.R. P. Singh, Physical Review B, **76** 184403 (2007).
 - ¹⁶ O. Cépas, C. M. Fong, P. W. Leung and C. Lhuillier, Phys. Rev. B **78**, 140405 (2008).
 - ¹⁷ L. Messio, O. Cépas and Lhuillier, C., Phys. Rev. B, **81**, 064428, (2010).
 - ¹⁸ J. S. Helton, K. Matan, M. P. Shores, E. A. Nytko, B. M. Bartlett, Y. Yoshida, Y. Takano, A. Suslov, Y. Qiu, J.-H. Chung, D. G. Nocera and Y. S. Lee, Phys. Rev. Lett. **98** 107204 (2007).
 - ¹⁹ J.S. Helton, K. Matan, M.P. Shores, E.A. Nytko, B.M. Bartlett, Y. Qiu, D.G. Nocera Y.S. Lee, Phys. Rev. Lett., **104** 147201 (2010).
 - ²⁰ T. H. Han, J. S. Helton, S. Chu, A. Prodi, D. K. Singh, C. Mazzoli, P. Müller, D.G. Nocera and Y. S. Lee, Phys. Rev. B, **83** 100402 (2011).
 - ²¹ J.-C. Domenge, P. Sindzingre, C. Lhuillier and L. Pierre, Phys. Rev. B, **72**, 024433 (2005)